The Design and Combustion Performance of Practical Swirlers for Integral Rocket/Ramjets

P. L. Buckley,* R. R. Craig,* D. L. Davis,* and K. G. Schwartzkopf*
U.S. Air Force Wright Aeronautical Laboratories, Wright-Patterson Air Force Base, Ohio

A method was devised for the design and fabrication of swirl inlet hardware with practical application to the integral rocket/ramjet dump combustor. A total of seven swirl inserts were tested to determine the effects of different swirl profiles on combustor performance. Combustor length-to-diameter ratio (L_c/D) was varied between 1.5 and 3, and the ratio of the nozzle throat to combustor area (A^*/A_3) between 40 and 60%. Combustor wall static distributions were measured in all configurations in which $L_c/D=3$. Airflow immediately downstream of the swirler was probed in cold flow to determine actual swirl angles to compare with prediction. Combustion instability data was recorded for subsequent spectral analysis by fast Fourier transform.

Nomencalature

A_3 = combustor area
A^* = nozzle throat area
c = blade chord length
C = velocity distribution constant
d = diameter at specified blade station
D = combustor diameter
F/A = fuel-air ratio
L_c/D = combustor length-to-diameter ratio
M_c = factor from Carter's deviation angle rule
N = number of blades
P = combustor pressure, kPa
P_{rms} = root mean square of pressure fluctuations
P_s = static pressure
P_t = total pressure
P_{t2} = combustor entrance total pressure
P_{t5} = nozzle throat total pressure
P_w = wall static pressure
r = radial position or radius, m
R = radius of blade curvature
R_1 = inner radius of swirler (center body radius)
R_2 = outer radius of swirler (inside radius of inlet)
s = distance between blades
S = swirl number
S_a^* = sonic air specific stream thrust, N/(kg/s)
T_t = total temperature
T_{ti} = ideal total temperature
T_{t2} = combustor entrance total temperature, K
T_{t5} = nozzle throat total temperature, K
T_{t5i} = ideal nozzle throat total temperature, K
u = axial velocity, m/s
w = tangential velocity, m/s
X = distance downstream of dump plane
γ = blade chord angle, deg
δ = deviation angle ($\phi-\theta$), deg
η_c = combustion efficiency
θ = airflow turning angle, deg
σ = solidity
ϕ = blade turning angle, deg

Introduction

THE use of swirl to improve the performance of turbojet augmentors has been developed in the last decade. However, it is only within the last few years that swirl has been considered in the efforts to increase the performance of integral rocket/ramjet combustors. Initial investigations in this area were very promising,[1,2] but the design tested was impractical for volume-limited missile applications. To be of practical value, any new swirl mechanism must be used in typical flameholder locations and operate at high subsonic velocities ($M=0.3$-0.5). Also, earlier test data did not conclusively demonstrate the high combustion efficiencies and low pressure losses expected of swirl addition relative to typical flameholder configurations.

With these considerations in mind, a study was conducted of several proposed[3] velocity profiles for swirling flows. To be consistent with previous work, a swirl number S of 0.4 was chosen as the baseline. Four specific swirl profiles were considered. These profiles were integrated from a center hub radius to the inlet radius to establish a tangential velocity profile. In an effort to decrease the swirler pressure losses, a circular arc blade was chosen, based on cascade research as reported in Ref. 4.

Design Procedure

The swirlers used in this work were of the axial flow variety, similar to the inlet guide vanes associated with axial flow turbines. All swirlers were designed to fit into a 10.2 cm inlet, approximately 10.2 cm upstream of the ramjet combustor. Each swirler consisted of 12 vanes, welded between a 10.2 cm i.d. outer ring and a 1.9 cm diam center body. The leading edge of each blade was aligned to be tangent to the incoming airflow and perpendicular to the inlet centerline. Because a circular arc blade was chosen, the desired turning angle at any given radial position could be obtained by simply extending the trailing edge as required. The actual design process consisted of three basic steps. First, the desired tangential velocity profile was determined as a function of radial position. Profiles chosen included constant angle, forced vortex, free vortex, and Rankine vortex as described in Ref. 3. Second, the desired degree of swirl was determined, characterized by the swirl number S. Finally, the blade geometry was chosen to give the desired profile.

The four tangential velocity distributions were specified as follows[3]:

Constant angle $$w=C_1 \quad (1)$$

Forced vortex $$w=C_2 r \quad (2)$$

Free vortex $$w=C_3/r \quad (3)$$

Rankine vortex $$w=\frac{C_4}{r}\left[1-\exp\left(\frac{-r^2}{R_2^2}\right)\right] \quad (4)$$

Presented as Paper 80-1119 at the AIAA 6th Aeroacoustics Conference, Hartford, Conn., June 30-July 2, 1980; submitted Feb. 19, 1982; revision received July 30, 1982. This paper is declared a work of the U.S. Government and therefore is in the public domain.

*Aerospace Engineer, Ramjet Technology Branch, Aero Propulsion Laboratory.

In order to provide a basis for comparison, all four profiles were tested with a common swirl number S defined as[3]

$$S=\int_{R_I}^{R_2} uwr^2\mathrm{d}r \Big/ R_2\int_{R_I}^{R_2} u^2 r\mathrm{d}r \tag{5}$$

The axial velocity was assumed to be constant, both across the inlet and on each side of the swirler, requiring that the swirl vanes accelerate the flow to provide the required tangential velocity component. Thus, with $u=$ const

$$S=\int_{R_I}^{R_2} wr^2\mathrm{d}r \Big/ \left[\frac{R_2 u}{2}\left(R_2^2-R_I^2\right)\right] \tag{6}$$

For the constant angle swirler, this reduces to a form identical to that used to describe a guide vane cascade in axial tube flow,[3]

$$S=\frac{2\left(R_2^3-R_I^3\right)}{3\left(R_2^3-R_2R_I^2\right)}\tan\theta \tag{7}$$

An axial velocity of 152.4 m/s was assumed initially, but because this is a constant velocity, this quantity may be combined with the tangential velocity distribution constants. After integration, the required airflow turning angle θ can be determined as a function of radial position. For the hardware chosen, and with $S=0.4$, the results were as follows with r in meters:

Constant angle $\theta=30.23$ deg (8)

Forced vortex $\theta=\tan^{-1}15.213r$ (9)

Free vortex $\theta=\tan^{-1}(0.02032/r)$ (10)

Rankine vortex $\theta=\tan^{-1}\left\{\frac{0.05338}{r}\left[1-e^{(-r^2/0.0026)}\right]\right\}$ (11)

The swirl vane geometry was developed from Carter's rule, based on experimental data obtained from two-dimensional cascades.[4] This procedure results in a simple method for determining the approximate blade angle required to achieve a given airflow turning angle.

The swirl vanes at a given radial positon may be represented in two dimensions as shown in Fig. 1. Carter's rule states

$$\delta/\phi=M_c/\sqrt{\sigma} \tag{12}$$

where M_c is a function of blade chord angle in degrees and may be approximated by

$$M_c=0.002\gamma+0.21 \tag{13}$$

The solidity σ is the ratio of blade chord length c to the distance between blade sections s.

The radius of curvature and the number of blades were specified initially. With these known quantities and the specified geometry, the chord length was determined such that $\theta-(\phi-\delta)=0$ in the following sequence:

$$\phi=2\gamma=2\sin^{-1}(c/2R) \tag{14}$$

From Carter's rule [Eq. (12)],

$$\sigma=c/s=cN/(\pi d) \tag{15}$$

where $d=$ the diameter at the specified blade station, and

$$\delta=\phi(0.002\gamma+0.21)/\sqrt{cN/(\pi d)} \tag{16}$$

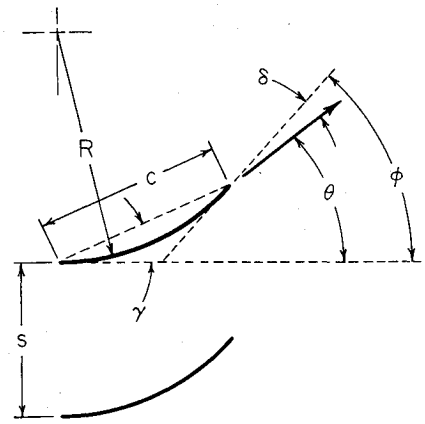

Fig. 1 Swirl vane geometry.

Combining

$$\theta\left(\frac{cN}{\pi d}\right)^{1/2}+\left(2\sin^{-1}\frac{c}{2R}\right)\left[0.21+0.002\sin^{-1}\frac{c}{2R}-\left(\frac{cN}{\pi d}\right)^{1/2}\right]=0 \tag{17}$$

This equation was solved numerically for c at each radial position. Note that angular units are in degrees. With c calculated, all other blade dimensions were determined. In order to minimize fabrication costs, all blades were stamped from 1.0 mm thick stainless steel sheet using a common die and trimmed to the appropriate outline. The leading edge of all blades was set perpendicular to the inlet centerline and the trailing-edge contour was determined by the turning angle required along the span of the blade. The radius of curvature at any given radial position was set equal to the distance from the inlet centerline. This resulted in an approximation of recommended values[5] of σ for all contours, which was intended to vary at 0.8-1.5 as ϕ varied at 15-40 deg.

Experimental Procedure

Combustor Models

The subscale ramjet test hardware, illustrated in Fig. 2, is of boiler plate construction as used for in-house parametric tests. The combustors were fabricated from 15.2 cm i.d. stainless steel pipe and weldneck flanges. Two lengths were used throughout the test series, one 45.7 cm long and one 22.9 cm, providing L_c/D (length-to-diameter) ratios of 3 and 1.5, respectively. In addition, one brief test series was accomplished with L_c/D equal to 1. Nominal combustor static pressure was measured at the ramjet nozzle entrance.

The ramjet nozzles used in these tests were water cooled with the internal liner machined from copper to form a convergent elliptical contour. Three throat diameters providing A^*/A_3 ratios of 0.4, 0.5, and 0.6 were tested.

Swirl Inlet

The swirl vane inserts were fabricated according to the design criteria described previously. A 10.2 cm long adapter section was bolted between the ramjet combustor and the 10.2 cm diam inlet normally used for our test work. The swirl inserts were mounted in this adapter, held in place by the inlet as shown in Fig. 2. Fuel injector fittings were mounted 3.8 cm upstream of the dump plane and 9.53 cm upstream of the swirl inlet adaptor. At each location, eight injectors could be inserted around the circumference. These injectors were designed to be used as wall injectors or could be moved inward toward the centerline as required. In addition, provisions were made to inject much further upstream to provide a premixed fuel air capability.

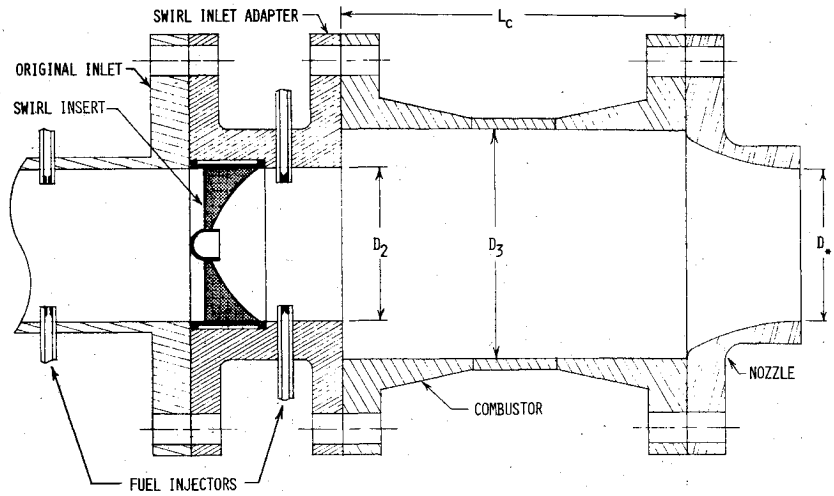

Fig. 2 Swirl inlet and combustor hardware.

Combustor Performance Calculations

The definition of combustion efficiency used throughout this paper is

$$\eta_c = \Delta T_t / \Delta T_{ti} \tag{18}$$

where ΔT_t is the total temperature rise across the combustor as computed from the thrust measurement, and ΔT_{ti} is the ideal total temperature rise for the measured fuel-air ratio (F/A) as computed from equilibrium chemistry calculations. Sonic air specific stream thrust S_a^* is obtained from the measured thrust by adding on the unbalanced ambient pressure forces and the exhauster suction forces acting on the hardware.[6]

In order for the Mod Comp II computer in the data acquistion system to calculate combustor performance as the tests are being conducted, certain equilibrium combustion properties must be available to it, namely, ideal total temperature rise, correlations of S_a^* vs combustor total temperature T_{t5}, and combustion gas specific heats. The only practical method of making these data available in a minicomputer is through a series of curve fits of the required properties.

Combustor ideal and actual total temperatures, T_{t5i} and T_{t5}, are determined from the measured values of F/A and S_a^*, respectively, by means of curve fits from the NASA-ODE equilibrium chemistry routine. Combustor total pressure ratios, P_{t5}/P_{t2}, are determined from measured static pressures, mass flow, and thrust, rather than from total pressure rakes. This method has been found to be more reliable and consistent than employing total pressure probes. The combustor inlet total pressure P_{t2} is computed from the measured inlet static pressure, mass flow, and total inlet temperature T_{t2}. The total pressure at the nozzle exit P_{t5} is computed from the nozzle throat area and the combustor total temperature, as calculated from the measured thrust.

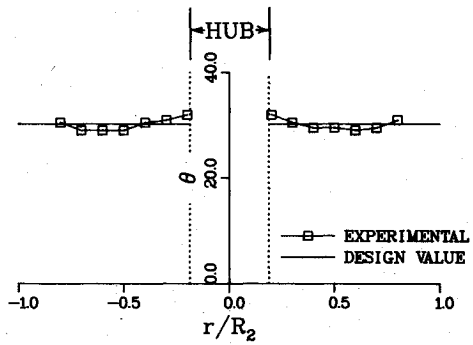

Fig. 3 Swirl angle profiles for constant angle swirler.

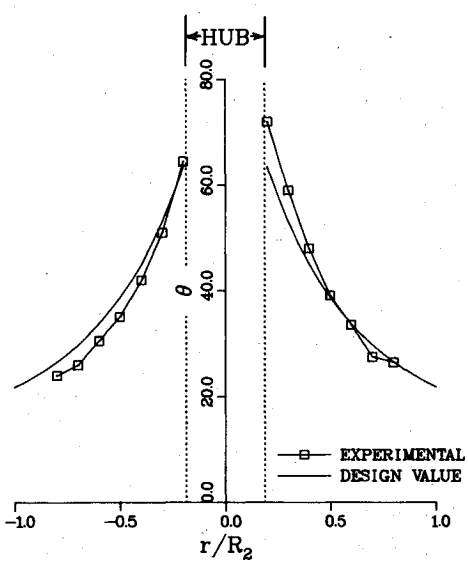

Fig. 4 Swirl angle profile for free vortex swirler.

Discussion and Results

Measured Swirl Profiles

Tests were conducted in cold flow to determine the actual flow angularity to compare with the predicted profiles for all swirlers. This was accomplished using a five-hole, three-dimensional, directional pitot probe inserted into the inlet through a fuel injection hole between the swirler and combustor. A reduced exit nozzle diameter was used to produce a chamber pressure and an inlet Mach number, upstream of the swirler, similar to those that occur during combustion. Results of two such tests may be seen in Figs. 3 and 4 for the constant angle (baseline) and free vortex swirlers. These profile measurements agree quite well with prediction, especially considering that deviation angles up to 14.5 deg were specified. This is the amount of blade turning angle required in excess of the desired airflow turning angle, as predicted by Carter's rule. The other constant angle swirlers also agreed closely with the predicted angles. Swirlers of the Rankine and forced vortex type provided slightly greater swirl than predicted near the center, indicating that these geometries may be more sensitive to interference from the hub.

Pitot-Static Profiles

Pitot-static profiles were measured at the inlet-to-combustor dump plane to obtain an indication of axial

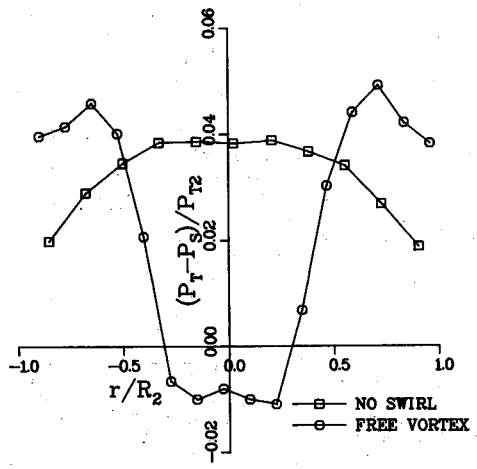

Fig. 5 Pitot-static profiles with and without swirl.

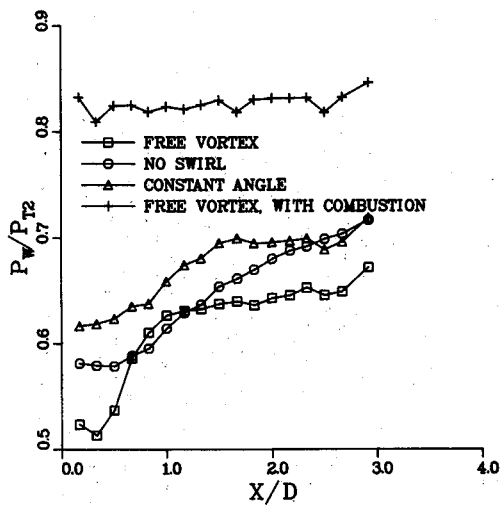

Fig. 6 Wall static pressure distribution.

velocity profiles using a Prandtl-type probe, positioned by a remote-operated traverse unit. Since the probe was aligned with the inlet and not with the flow, measurements for the swirl cases should be compared on a qualitative basis only. Two of these profiles are shown in Fig. 5, one with no swirl and the other with the free vortex swirler. The data with no swirl show a typical well-developed turbulent pipe flow. The free vortex profile was chosen to illustrate the most predominant case observed with flow reversal in the center of the inlet area. All three constant angle swirlers ($S=0.3$, 0.4, 0.5) generated a zone of reverse flow with the 0.5 case resulting in a profile very similar to that of the free vortex. The pitot-static profiles measured for the forced and Rankine vortex swirlers show areas of decreased axial velocity near the centerline, but not of sufficient magnitude to indicate a central recirculation zone.

Combustor Static Pressure Distribution

Wall static pressure taps were distributed at 2.5 cm increments downstream of the dump plane for the length of the baseline combustor ($L_c/D=3$). Pressure distributions were recorded prior to combustion and at each of the selected F/A ratios at which combustion performance was recorded.

Wall static pressure distributions are shown in Fig. 6 for the cases of no swirler, the free vortex swirl generator, and the constant angle swirl generator, both designed to produce a swirl number of 0.4. With no swirler, the wall static pressure continues to rise for the entire length of the chamber, even though flow reattachment occurs at about the midpoint of the

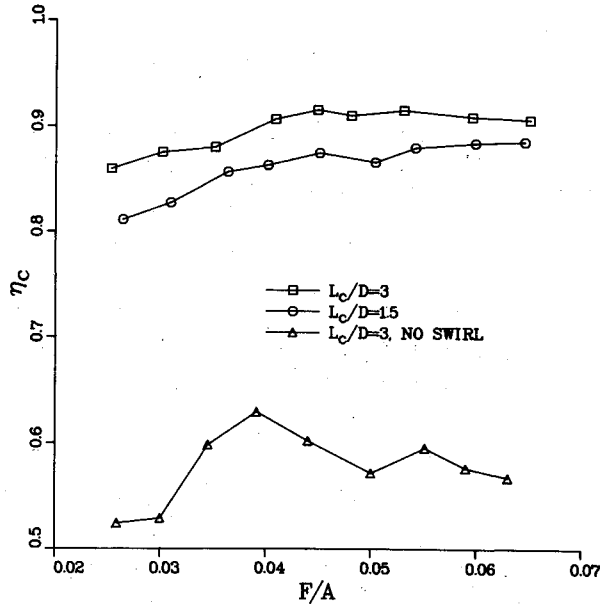

Fig. 7 Baseline swirler performance.

chamber for the 2.5 cm step at the combustor entrance. For the constant angle swirler, the wall static pressure levels off about 25.4 cm from the dump and for the free vortex swirler, this leveling off of the pressure distribution occurs at about 15.2 cm from the dump plane. This is a very positive indication of the drastic reduction of the wall recirculation zone length caused by high degrees of swirl.

With combustion, the wall static pressure distributions become essentially constant and it is not possible to discern from the distributions if there was a swirl generator in the flow or not.

Comparison of the computed combustor total temperature from the thrust measurement and the wall static pressure measurement just upstream of the sonic nozzle can provide useful information on the effects of residual swirl at the combustor exit. Differences should arise since swirl increases static wall pressures and decreases thrust because of the angular velocity component.

With no swirl and no combustion, the thrust measurement yields the correct one-dimensional average gas temperature, whereas the static pressure yields a value 10% too low since the flow has not completely redeveloped to a uniform state after the sudden expansion at the combustor entrance. For the constant angle swirler with $S=0.4$ and no combustion, gas temperature computed from thrust is 5% low and the pressure computed value is 23% too high.

With combustion and the same swirler at a lean F/A ratio of 0.0259, the pressure computed temperature is 4% lower than the thrust computed value and at a F/A ratio of 0.063, the computed temperatures are within 1% of each other.

From this comparison, one can conclude that with combustion, losses in thrust due to residual swirl, at least to the sonic point of the nozzle, are negligible.

Baseline Combustor Tests

Initially, the baseline configuration was defined with a combustor L_c/D of 3 under the assumption that the longer combustor would be required for stable operation throughout most test conditions. However, after initial tests to establish the optimum fuel injection scheme, it was possible to operate the shorter chamber over all conditions with only a slight decrease in performance. Thus, two parallel baselines were established with all test variables applied to each. The remaining details of each baseline include a 50% nozzle area ratio, airflow of 1.8 kg/s, inlet temperature of 555 K, and the constant angle swirler with a swirl number of 0.4.

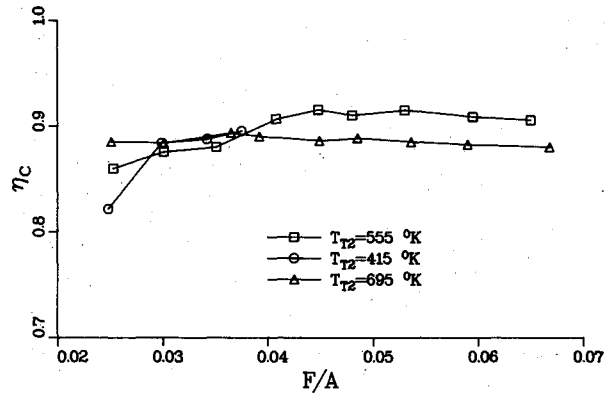

Fig. 8 Effect of inlet air temperature on baseline swirler performance, $L_c/D=3$.

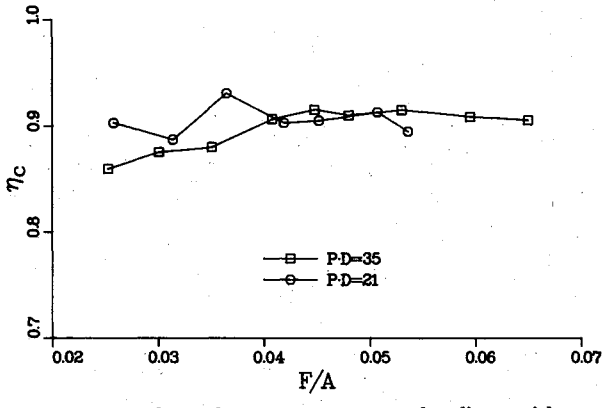

Fig. 9 Effect of combustor pressure on baseline swirler performance, $L_c/D=3$.

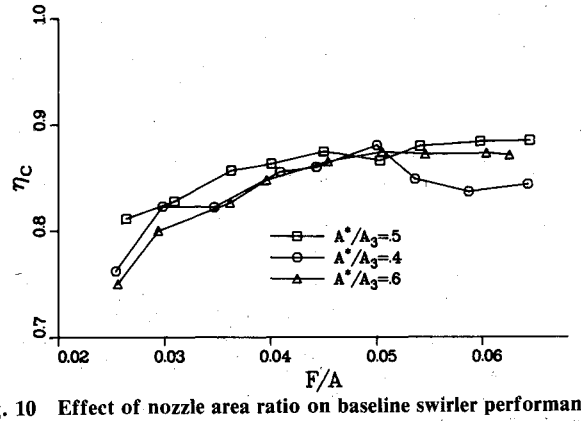

Fig. 10 Effect of nozzle area ratio on baseline swirler performance, $L_c/D=1.5$.

After initial experimentation, the fuel injection configuration used for all tests consisted of eight injectors with 1.17 mm diam orifices mounted 9.5 cm upstream of the swirl inlet adaptor. Four were inserted to a depth of 6.4 mm from the inlet wall and four were inserted 9.5 mm.

The combustion efficiencies of the two baseline configurations are compared in Fig. 7. Very similar operating characteristics were observed with only a 3-5% loss in combustion efficiency for the short chamber. Also included in this plot is the long baseline combustor performance with no swirl. The improved performance of the long combustor with swirl resulted in no loss of pressure recovery due to swirl addition. The average pressure recovery of each was approximately 88%.

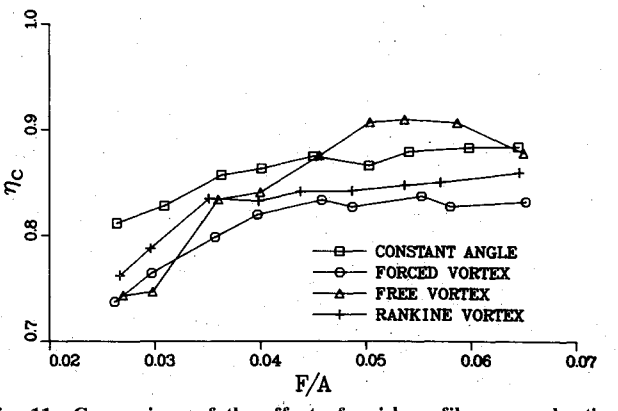

Fig. 11 Comparison of the effect of swirl profile on combustion efficiency, $L_c/D=1.5$.

Inlet Temperature Effects

The baseline inlet temperature was established as 555 K for all configurations. The effect of varying this temperature from 415 to 695 K can best be seen for the long chamber baseline shown in Fig. 8. Little performance improvement was obtained by increasing the inlet temperature. At the lower temperature, combustion efficiency decreased 3-4% and the operating range of the combustor was limited to F/A ratios of 0.025-0.045. The rich blowout could possibly have been increased with different fuel placement, as the injection configuration was optimized for operation at 555 K baseline test conditions.

A similar rich blowout was encountered for the short chamber baseline at the lower inlet temperature. At 695 K, a slight decrease in performance was noted, again perhaps due to fuel injection. These trends continued throughout all other test configurations.

Combustion Pressure and Velocity Effects

The baseline air mass flow of 1.8 kg/s was chosen to conform to "pressure-diameter" scaling criteria of $P\cdot D=35.0$ kPa·m to be consistent with earlier in-house work.[6] Operation at $P\cdot D=21.0$ kPa·m is compared for the long chamber baseline in Fig. 9. In general, lower pressure operation resulted in a slightly limited F/A operating range and, in the short combustor, a combustion efficiency decrease of 1-5%.

By changing the nozzle throat area A^* and varying the airflow to maintain a constant combustor pressure, it was possible to operate with different combustor velocities. Figure 10 compares operation with a 40 and a 60% area ratio nozzle, resulting in both a 20% decrease and increase in combustor velocity. Little change is noted in combustor performance. This is characteristic of all configurations tested with the single exception of the long combustor baseline. In that particular case, stable combustion could not be attained with the 40% nozzle due to a large-amplitude low-frequency instability.

Comparison of Four Swirl Profiles

Four swirl profiles were tested with a common calculated swirl number of 0.4. These were the constant angle, forced vortex, free vortex, and Rankine vortex, as described in the design procedure.

The performance of these four swirl profiles is compared in Fig. 11 as tested with the short chamber baseline. The free vortex provided the highest peak efficiency, dropping off at lower fuel-air ratios, while the best overall performance is attained with the constant angle swirler. In the case of the long chamber baseline, the free vortex swirler provided the highest combustion efficiency over the entire operating range,

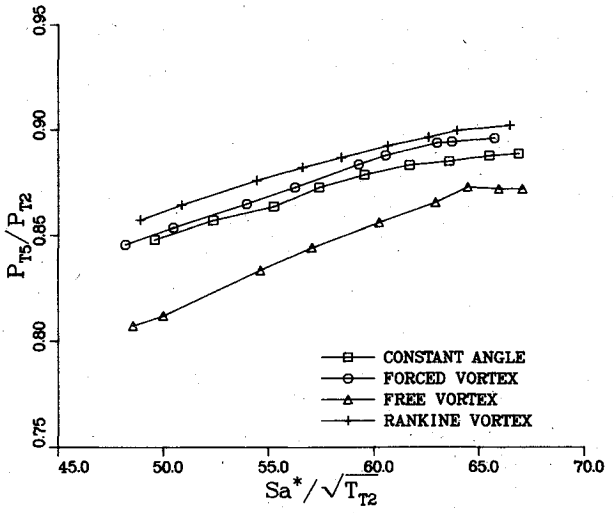

Fig. 12 Combustor pressure recovery of various swirl generators, $L_c/D=1.5$.

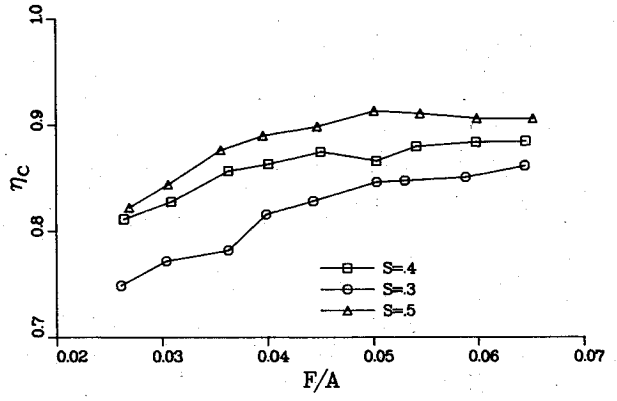

Fig. 13 Effect of swirl number on baseline swirler performance, $L_c/D=1.5$.

peaking at approximately 95%. In general, the long chamber produced higher overall efficiencies with less degradation at the lower fuel-air ratios.

The pressure recoveries for these four swirl profiles are compared for the short chamber baseline in Fig. 12. As seen in this plot, the high combustion efficiency obtained with the free vortex swirler is gained at the cost of a slightly greater pressure loss. Pressure recoveries obtained for each swirler in the long baseline combustor were about 1% greater than those obtained in the short baseline combustor tests.

Comparison of Three Swirl Numbers

Up to this point, all swirlers were designed to provide a swirl number of 0.4 in order to evaluate the merits of each profile. As previously stated, 0.4 was chosen based on earlier work and recommendations.[1,2] Whether or not this was really an optimum value was unknown. For this reason, constant angle swirlers with calculated swirl numbers of 0.3 and 0.5 were fabricated and tested to allow a direct comparison to the baseline hardware. The performance of these swirlers is shown in Fig. 13 relative to the short baseline. Maximum performance is obtained with $S=0.5$ with η_c peaking at 91.4% for a F/A ratio of 0.050. Results with the long chamber baseline were characterized by very similar efficiencies at $S=0.3$ and 0.4, running from $\eta_c \simeq 0.86$ at F/A of 0.025 to $\eta_c \simeq 0.90$ at F/A of 0.065. The 0.5 swirler tested with the long chamber yielded combustion efficiencies in excess of 0.90 across the entire F/A range. It is interesting to note that for F/A ratios above 0.045, there is less than 2% difference in

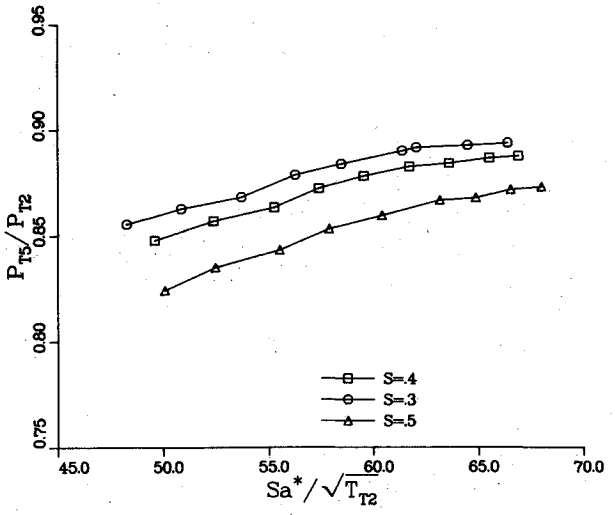

Fig. 14 Effect of swirl number on baseline swirler combustor pressure recovery, $L_c/D=1.5$.

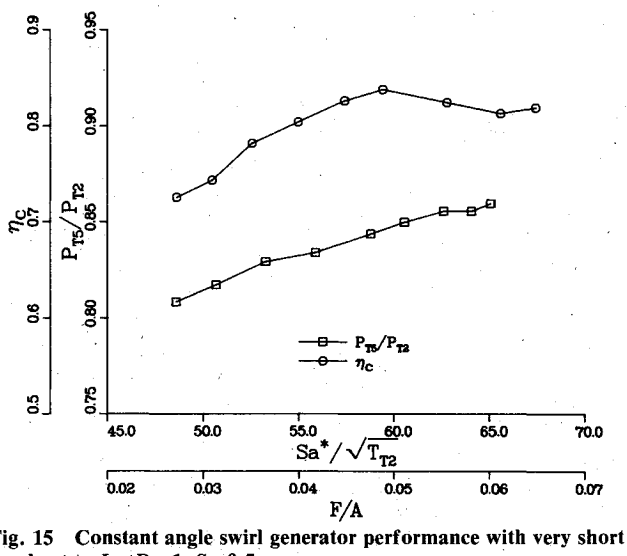

Fig. 15 Constant angle swirl generator performance with very short combustor, $L_c/D=1$, $S=0.5$.

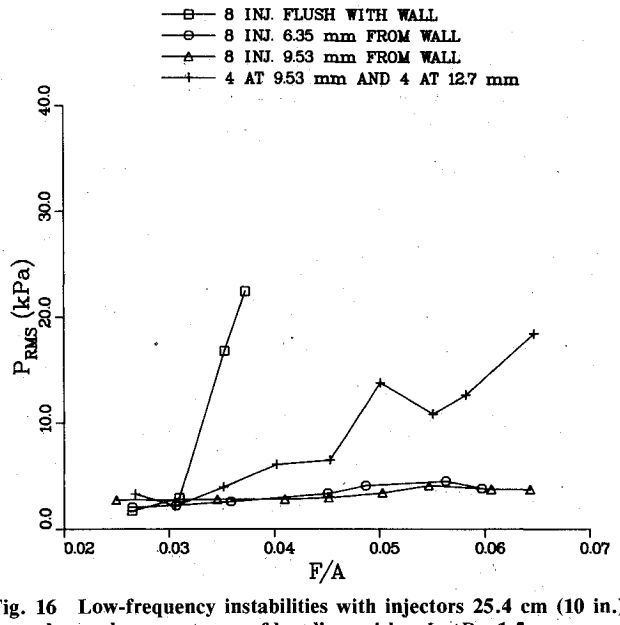

Fig. 16 Low-frequency instabilities with injectors 25.4 cm (10 in.) from dump plane, upstream of baseline swirler, $L_c/D=1.5$.

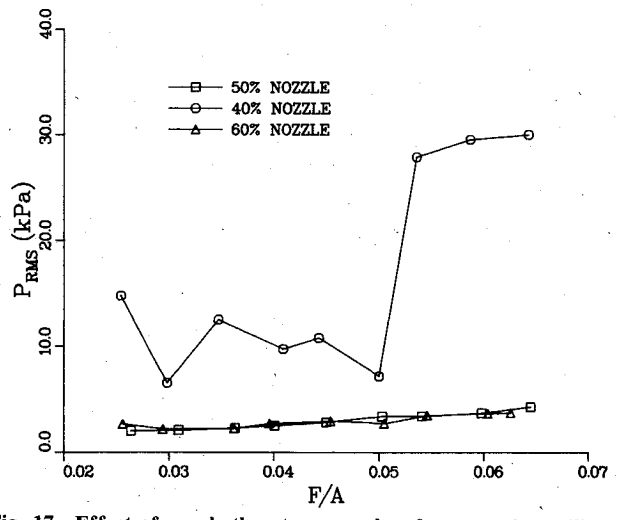

Fig. 17 Effect of nozzle throat area on low-frequency instabilities, baseline swirler.

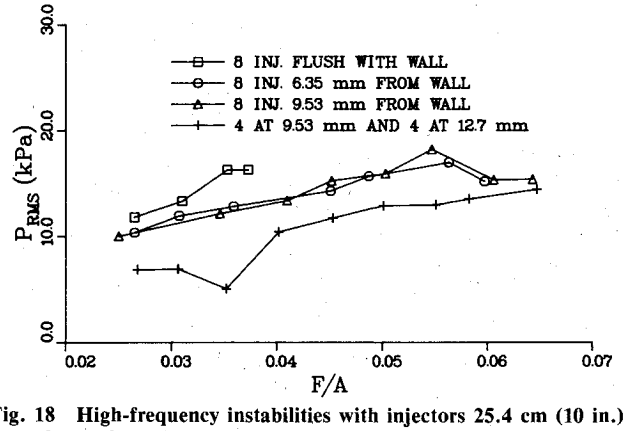

Fig. 18 High-frequency instabilities with injectors 25.4 cm (10 in.) from dump plane, upstream of baseline swirler, $L_c/D = 1.5$.

combustion efficiency between the long and short chamber with a swirl number of 0.5. The pressure recovery for the three swirl numbers is shown in Fig. 14 for the short chamber. Pressure recoveries obtained in the long combustor were about 1-2% higher than the values obtained in the short combustor.

Shortened Chamber Tests

With the encouraging results obtained at an L/D of 1.5, the next task was to experiment with a shorter chamber. In Fig. 15 both combustion efficiency and pressure recovery are plotted for a chamber length of 15.2 cm, providing an L_c/D of 1.0. The constant angle swirler was installed for this test with a swirl number of 0.5. As shown, peak combustion efficiency was measured as approximately 84% with a pressure recovery range of 81-86%. Optimization of the fuel injection distribution was not attempted for this case as it was for L_c/D of 1.5.

Combustion Instabilities

The combustion induced pressure oscillations that occurred in these tests, as measured 7.6 cm downstream of the dump, were divided into three groups:

Very low frequencies (chugging)	0-100 Hz
Low frequencies (rumble)	100-1000 Hz
High frequencies (screech)	1000-10,000 Hz

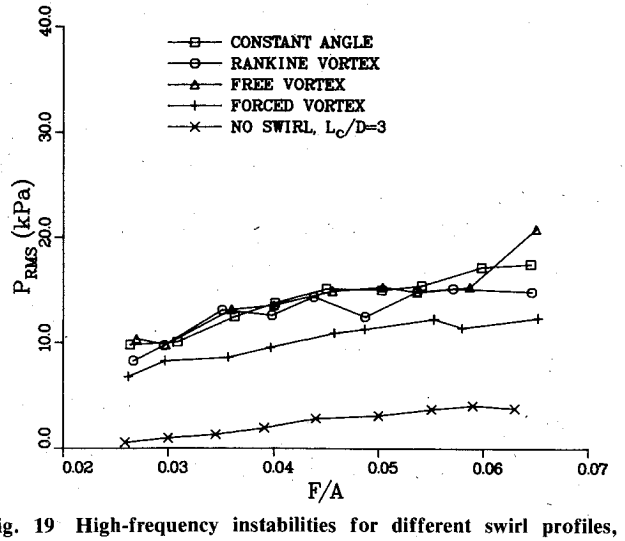

Fig. 19 High-frequency instabilities for different swirl profiles, $S = 0.4$, $L_c/D = 1.5$.

All instability amplitudes in this report are total rms pressures over the entire range of each frequency group as obtained with a Nicolet 660A fast Fourier transform analyzer.[7,8] These pressures include harmonics of discrete instabilities as well as apparently indiscrete oscillations. Rms pressures also approximate one-fourth of the peak-to-peak pressure observed in the time domain.[9]

The pressure in the combustion chamber was held at about 207 kPa during combustion. An approximation of peak-to-peak pressure over chamber pressure can be obtained by multiplying the total rms pressure by 0.017 to 0.023 kPa^{-1}.

Low-Frequency Oscillations

Fuel distribution had a pronounced effect on observed low-frequency combustion instabilities. During initial swirl testing, the radial position of the fuel injectors was varied in order to obtain high combustion efficiency over the entire operating range of the combustor. With the injectors 10.2 cm upstream of the swirler, low-frequency oscillations were observed with the injectors flush (400 Hz) and at the most inward radial position (300 Hz), see Fig. 16.

Smaller nozzle throat areas have been found to be associated with low-frequency combustion instabilities. With the short combustor baseline swirl configuration, only low-amplitude (300 Hz, 4 rms kPa), low-frequency instabilities were observed, while with a smaller nozzle throat ($A^*/A_3 = 40\%$) high amplitude, low-frequency oscillations (300 Hz, 30 rms kPa) occurred, see Fig. 17.

High-Frequency Instabilities

High-frequency combustion instabilities occurred consistently throughout the testing of the swirl hardware. Fuel injection (Fig. 18) and type of swirler (Fig. 19) had little effect on the amplitude of high-frequency instabilities.

The amplitude of the high-frequency instabilities increased with the fuel-air ratio. The primary frequency of the high-frequency instabilities, which appear to be first-order tangential mode instabilities, varies from 3000 Hz at the high fuel-air ratios to 2500 Hz at low fuel-air ratios.

Conclusion

This work has clearly shown the high performance which can be obtained by the addition of swirl to the ramjet dump combustor. Compared to typical flameholders tested previously,[10] this performance benefit was accompanied by significantly lower pressure losses.

In order to design and fabricate the swirl hardware, relatively simple methods were developed to determine the

required turning angle for a given swirl number and profile. Also, experimental cascade data were applied to the swirl vane design in order to establish the vane turning angle required for a given airflow turning angle. These procedures could be improved by a more exact analysis of the desired tangential velocity profiles and by application of more involved turbojet design procedures for blades.

It would be very difficult to choose a single swirler tested as being clearly superior to the others. The forced vortex and Rankine vortex swirlers deviated slightly from the desired velocity profiles and did not perform quite as well. The free vortex swirler provided the best peak efficiency for $S=0.4$, but with slightly greater pressure loss. The constant angle swirlers were very straightforward in design and agreed closely with predicted turning angles. Very good performance was obtained with this baseline profile with greater combustion efficiencies made possible by increasing the swirl number, at the expense of some pressure recovery.

All of these swirl generators were inserted into a typical ramjet inlet, providing improved performance with little modification to the inlet configuration.

Low-frequency instabilities that occurred in preliminary combustion testing disappeared, for most cases, in the process of fuel injection development. In almost every combusting condition with swirl, a high-frequency combustion instability was observed, but the amplitudes were insufficient to arouse any particular concern as to their destructive nature.

Additional data, hardware description, and analysis may be found in Ref. 10.

References

[1] Quinn, R. E., "Research and Development on Short Ramjet Dump Combustors," AFAPL-TR-77-91, Dec. 1977.

[2] Buckley, P. L., Craig, R. R., and Obleski, B. M., "The Effect of Swirl on a Ramjet Dump Combustor," AIAA Paper 79-7042, April 1979.

[3] Beér, J. M. and Chigier, N. A., *Combustion Aerodynamics,* Halstead Press Div., John Wiley & Sons, New York, 1972, pp. 100-146.

[4] "Aerodynamic Design of Axial-Flow Compressors," NASA SP-36, 1965.

[5] Wennerstrom, A. J., Private communication, Air Force Aero Propulsion Laboratory, Wright-Patterson AFB, Ohio, March 1979.

[6] Craig, R. R., Buckley, P. L., and Stull, F. D., "Large Scale, Low Pressure Dump Combustor Performance," AIAA Paper 75-1303, Sept. 1975.

[7] "Understanding Dual Channel FFT Measurements, Cause and Effect Relationships," Nicolet Scientific Corp., Northvale, N. J., Fall 1978.

[8] "Instruction Manual for Model 660 Dual-Channel FFT Analyzer," Nicolet Scientific Corp., Northvale, N.J., 1978.

[9] Beranek, L. L., *Noise and Vibration Control,* McGraw-Hill Book Co., New York, 1971, pp. 11-12 and 36-40.

[10] Buckley, P. L., Craig, R. R., Davis, D. L., and Schwartzkopf, K. G., "The Design and Combustion Performance of Practical Swirlers for Integral Rocket/Ramjets," AIAA Paper 80-1119, June 1980.